Radiative damping and electron beam dynamics in plasma-based accelerators

P. Michel, C. B. Schroeder, B. A. Shadwick, E. Esarey,* and W. P. Leemans*
Lawrence Berkeley National Laboratory, Berkeley, California 94720, USA
(Received 27 April 2006; published 15 August 2006)

The effects of radiation reaction on electron beam dynamics are studied in the context of plasma-based accelerators. Electrons accelerated in a plasma channel undergo transverse betatron oscillations due to strong focusing forces. These oscillations lead to emission by the electrons of synchrotron radiation, with a corresponding energy loss that affects the beam properties. An analytical model for the single particle orbits and beam moments including the classical radiation reaction force is derived and compared to the results of a particle transport code. Since the betatron amplitude depends on the initial transverse position of the electron, the resulting radiation can increase the relative energy spread of the beam to significant levels (e.g., several percent). This effect can be diminished by matching the beam into the channel, which could require micron sized beam radii for typical values of the beam emittance and plasma density.

DOI: 10.1103/PhysRevE.74.026501 PACS number(s): 41.60.Ap, 41.75.Ht, 52.40.Mj

I. INTRODUCTION

Over the last few years, plasma-based accelerator [1] research has achieved major results. In particular, quasimonoenergetic electron beams in the 100 MeV range have been obtained from laser wakefield accelerators [2–4], while plasma wakefield accelerators have demonstrated electron energy gains in the multi-GeV range [5]. In addition to the enormous accelerating gradients associated with the plasma wave (wakefield), which can be on the order of 10–100 GV/m, the transverse focusing forces are also extremely strong and can be on the order of the accelerating force. Hence, the electrons that get trapped and accelerated in the plasma focusing channel of the wakefield can undergo strong transverse betatron oscillations. These oscillations give rise to the emission of intense synchrotron radiation, which has been recently studied theoretically [6] and demonstrated experimentally for both laser-driven [7,8] and beam-driven [9,10] plasma accelerators.

Since the amount of energy that goes from the electrons into the betatron radiation can be substantial, it may have a significant effect on the evolution of the electron beam properties. A primary effect is a decrease of the electron beam energy due to the emission of radiation [11,12]. This in turn will affect the energy-dependent betatron frequency, as well as the other beam properties, such as the energy spread and emittance.

The synchrotron radiation process can be used to cool electrons, as can be the case for an electron beam passing through an undulator magnet [13]. An important parameter characterizing the synchrotron radiation from an undulator magnet is the undulator strength parameter $a_u = eB_u/(k_u mc^2)$, where B_u is the amplitude of the undulator magnetic field, $\lambda_u = 2\pi/k_u$ is the undulator period, e is the electron charge, m is the electron mass, and c is the speed of light in vacuum. For example, the power radiated by a single electron in an undulator field scales as $P_u \sim \gamma^2 k_u^2 a_u^2$, where γ is the relativistic factor of the electron. Since higher energy electrons (higher γ) radiate more than lower energy electrons, the electron energy spread will decrease as the electrons radiate in an undulator field, which is often referred to as electron cooling or radiative damping. Several electron cooling schemes have been used or proposed that use a variety of methods to cause the electrons to oscillate and radiate, such as bending magnets [13], crystal channels [14], and laser fields [15–18].

The electron beam dynamics in a plasma focusing channel is intrinsically different from that in a conventional undulator magnet. In an ideal undulator field, all of the electrons experience an axially periodic transverse magnetic field that is approximately constant as a function of radius. This causes the transverse momentum oscillations p_u of the electrons to all have approximately the same amplitude, $p_u = mca_u$, independent of the initial radial position of the electron. This is not the case for a plasma focusing channel, since the radial focusing force of the wakefield is a strong function of radius (i.e., the radial focusing force is typically linear with radius near the axis). Hence, the transverse motion of an electron is a strong function of the initial radial position of that electron. For example, in an ideal wakefield, an electron injected on axis will travel in a straight line along the axis, whereas an electron residing off axis will exhibit a large transverse oscillation. The betatron strength parameter, characterizing the betatron radiation, is $a_\beta = \gamma k_\beta r_\beta$, where $\lambda_\beta = 2\pi/k_\beta$ is the betatron period and r_β is the radial amplitude of the betatron oscillation. One consequence is that an electron traveling along the axis will not loose energy due to betatron emission, whereas an off-axis electron with a large betatron amplitude could loose significant energy. Hence, betatron emission in a plasma focusing channel can result is an increase in electron energy spread. However, although the relative energy spread will increase for a finite radius electron beam injected on axis, it still may be possible for the normalized emittance to decrease as a result of betatron radiation.

The paper is organized as follows. The case where relativistic electrons are injected into a straight, focusing plasma channel in the absence of longitudinal acceleration is analyzed in Sec. II. Using a separation of time scales, analytical results are derived for both the single particle orbits and the beam moments including radiation reaction. In Sec. III, modifications due to the addition of a uniform longitudinal

*Also at University of Nevada, Reno.

 ©2006 The American Physical Society

accelerating field are considered. Section IV presents simulation results for the case where the axial and transverse fields are those obtained from linear plasma wakefield theory. Several examples relevant to plasma accelerators are given, including those in which the effects of radiation are potentially detrimental if not properly controlled. Also included are two appendices that describe some mathematical details regarding the mean energy and energy spread, as well as an analysis of mismatched beams, including a calculation of the decoherence time and emittance growth.

II. CONSTANT FOCUSING CHANNEL

Consider, in (x,z) slab geometry, an electron beam moving along the z axis in a constant, axially uniform focusing channel. In this section, we will neglect the axial electric field and assume the transverse field is that produced by a quadratically varying potential

$$\phi(x) = \phi_0(1 - x^2/x_c^2), \tag{1}$$

where x is the transverse displacement from axis, x_c is the characteristic channel width, and ϕ_0 sets the strength of the potential. In the focusing channel the electron momentum evolves according to

$$\frac{du_x}{dct} = -K^2 x + F_x^{\mathrm{RAD}}/mc^2, \tag{2}$$

$$\frac{du_z}{dct} = F_z^{\mathrm{RAD}}/mc^2, \tag{3}$$

where $\boldsymbol{F}^{\mathrm{RAD}}$ is the radiation reaction force and $\boldsymbol{u}=\boldsymbol{p}/mc$ is the normalized electron momentum, with m the mass of the electron and c the speed of light. It is convenient to parametrize the transverse focusing force in terms of the "spring-constant" $K^2=2x_c^{-2}(e\phi_0/mc^2)$, where $-e$ is the electronic charge. Note that in the blow-out regime, in which the focusing force is determined by a bare, uniform ion column, $K=k_p/\sqrt{2}$ (cf. Ref. [6]), where $\omega_p=ck_p=(4\pi n_0 e^2/m)^{1/2}$ is the plasma frequency and n_0 is the ambient plasma density.

The classical expression of the radiation reaction force is [19]

$$\frac{\boldsymbol{F}^{\mathrm{RAD}}}{mc\tau_R} = \frac{d}{dt}\left(\gamma\frac{d\mathbf{u}}{dt}\right) + \gamma\mathbf{u}\left[\left(\frac{d\gamma}{dt}\right)^2 - \left(\frac{d\mathbf{u}}{dt}\right)^2\right], \tag{4}$$

where $\gamma=(1+u^2)^{1/2}$ is the relativistic Lorentz factor of the electron and $\tau_R=2r_e/3c\simeq 6.26\times 10^{-24}$ s with $r_e=e^2/mc^2$ is the classical electron radius. Assuming the length scale associated with this force $c\tau_R$ is much smaller than the scale length of the betatron motion, we may treat the radiation reaction force as a perturbation. Thus we evaluate the radiation force using the unperturbed orbits [i.e., using Eqs. (2) and (3) with $\boldsymbol{F}^{\mathrm{RAD}}=0$]. This approximation yields

$$F_x^{\mathrm{RAD}} \simeq -mc^3\tau_R K^2 u_x(1 + K^2\gamma x^2), \tag{5}$$

$$F_z^{\mathrm{RAD}} \simeq -mc^3\tau_R\gamma^2 K^4 x^2, \tag{6}$$

where we have made the additional assumption that $u_z \gg u_x$. The equations of motion are then

$$\dot{u}_x \simeq -cK^2 x - c^2\tau_R K^2 u_x(1 + K^2\gamma x^2), \tag{7}$$

$$\dot{u}_z \simeq -c^2\tau_R K^4\gamma^2 x^2, \tag{8}$$

and $\dot{x}=cu_x/\gamma$, where the dot notation denotes a time derivative. We expect this perturbation (radiation reaction force much less than the Lorentz force) to be valid provided $c\tau_R K/\gamma_0^{1/2} \ll 1$. Note that the semiclassical treatment of the radiative effects requires the Compton wavelength $\lambda_C=h/mc$ to be much less than the radiation wavelength in the electron rest frame, i.e., $\lambda_C \ll 2\gamma\lambda_{\mathrm{rad}}$. For $a_\beta^2 \gg 1$, this condition becomes $\lambda_C \ll \lambda_\beta/(\gamma a_\beta)$.

A. Single particle dynamics

1. Particle orbits without radiation

In the absence of the radiation reaction force, the electron orbits are given by $\dot{x}=cu_x/\gamma$, $\dot{u}_x=-cK^2x$, and $\dot{u}_z=0$. The following initial conditions are assumed: $x(t=0)=x_0$, $u_x(t=0)=u_{x0}$, $\gamma(t=0)=\gamma_0$ (except when otherwise specified, the zero subscript refers to the value at the initial time through the rest of the paper). As in Ref. [6], the particle orbits simply follow a harmonic oscillation in the transverse direction at the betatron frequency $\omega_\beta=ck_\beta=Kc/\gamma_0^{1/2}$. Furthermore, since $\dot{x}(t=0)=cu_{x0}/\gamma_0$ and $\dot{u}_x(t=0)=-cK^2x_0$, the electron orbits are

$$x = x_0\cos\omega_\beta t + \frac{u_{x0}}{k_\beta\gamma_0}\sin\omega_\beta t, \tag{9}$$

$$u_x = u_{x0}\cos\omega_\beta t - x_0 k_\beta\gamma_0\sin\omega_\beta t. \tag{10}$$

The transverse orbit Eq. (9) can also be written in the form $x=x_m\cos(\omega_\beta t+\delta)$, with amplitude $x_m^2=x_0^2+u_{x0}^2/(k_\beta^2\gamma_0^2)$ and phase $\delta=-\arctan[u_{x0}/(x_0k_\beta\gamma_0)]$.

2. Energy damping

An expression for the radiative damping rate can be derived by assuming that $\gamma\simeq u_z$ in Eq. (8), i.e.,

$$\dot{\gamma} = -\tau_R c^2 K^4 x^2\gamma^2. \tag{11}$$

Since the effect of the radiation on the transverse oscillation amplitude is treated as a perturbation, and since the time scale for radiation damping is long compared to the betatron period, Eq. (11) can be time averaged, i.e., $\langle x^2\rangle_t \simeq x_m^2/2$, which gives

$$\gamma = \frac{\gamma_0}{1 + \nu_\gamma t}, \tag{12}$$

with the radiative damping rate

$$\nu_\gamma = \tau_R c^2 K^4 x_m^2\gamma_0/2. \tag{13}$$

Alternatively, in terms of the betatron strength parameter [6], defined as $a_\beta=k_\beta\gamma_0 x_m$, the damping length, defined as $L_d=c/\nu_\gamma$, is $L_d=(c\tau_R\gamma_0 a_\beta^2 k_\beta^2/2)^{-1}$. This result is analogous to the result for the case of radiation damping via Thomson scattering, only with a_β and k_β replaced by the laser strength

parameter and laser wave number, respectively [18].

The differences in the definition of the strength parameters illustrates some of the fundamental differences that exist between laser-Thomson scattering and a plasma-focusing channel. For Thomson scattering, cooling is effective when the spot size of the laser is large compared to the radius of the electron beam. In this case, the laser strength parameter a_0 (which is the normalized vector potential of the laser, $a_0=eA_0/mc^2$ where A_0 is the maximum amplitude of the vector potential) is approximately independent of radial position. In contrast, for a focusing channel, the betatron strength parameter is linearly proportional to the amplitude of the transverse oscillation of the electron, which is a strong function of the initial radial position of the electron. For example, an electron injected on the axis with no transverse momentum will move straight along the channel axis, without any oscillation and hence without any damping. On the other hand, the damping will be much stronger for particles injected farther from axis.

Alternatively, the radiative damping rate can be derived by considering the power radiated by a moving charge, which in the classical limit is [19]

$$P_s = \frac{2e^2}{3c}\gamma^2\left[\left(\frac{d\mathbf{u}}{dt}\right)^2 - \left(\frac{d\gamma}{dt}\right)^2\right]. \tag{14}$$

Using $mc\dot{\gamma}=\mathbf{F}_{\text{ext}}\cdot\mathbf{u}/\gamma$, where $\mathbf{F}_{\text{ext}}$ is the external force on the electron, gives

$$P_s = \frac{2e^2\gamma^2}{3m^2c^3}[|\mathbf{F}_{\text{ext}}|^2 - |\mathbf{F}_{\text{ext}}\cdot\boldsymbol{u}/\gamma|^2]. \tag{15}$$

When the force is transverse only, $\mathbf{F}_{\text{ext}}=F_\perp\mathbf{e}_\mathbf{x}$, and for a relativistic electron with $u_x^2 \ll \gamma^2$, the radiated power can be written

$$P_s \simeq \frac{2e^2\gamma^2}{3m^2c^3}F_\perp^2. \tag{16}$$

The characteristic damping time can be defined as the ratio of the radiated power to the electron energy, $\nu_\gamma=P_s/\gamma mc^2$, which yields the radiative damping rate [20,21] $\nu_\gamma=\tau_R\gamma F_\perp^2/m^2c^2$. Substituting the transverse force from the plasma focusing channel, $F_\perp=-mc^2K^2x$, and time averaging over a betatron oscillation, yields Eq. (13).

3. Particle orbits with radiation

Assuming $\gamma\simeq u_z$, Eqs. (7) and (8) can be recast into a coupled set of equations,

$$\ddot{x} + \tau_R c^2K^2\dot{x} + K^2c^2x/\gamma = 0, \tag{17}$$

$$\dot{\gamma} = -\tau_R c^2K^4x^2\gamma^2. \tag{18}$$

The position-independent damping term in Eq. (17), $\tau_R c^2K^2\dot{x}$, is small and can be neglected. It is convenient to introduce the normalized variables $X=x/x_m$, $\Gamma=\gamma/\gamma_0$, $\tau=\omega_\beta t$, and $\epsilon=\nu_\gamma/\omega_\beta$, such that Eqs. (17) and (18) can be rewritten

$$X'' + \Gamma^{-1}X = 0, \tag{19}$$

$$(\Gamma^{-1})' = 2\epsilon X^2, \tag{20}$$

where the prime notation designates the derivative with respect to τ.

To solve Eqs. (19) and (20), we consider a separation of time scales: The fast betatron oscillations of the order ω_β^{-1} and the slow radiation damping of the order ν_γ^{-1}, such that $\epsilon=\nu_\gamma/\omega_\beta \ll 1$. Consider a perturbation series in ϵ such that $X\simeq X^{(0)}+\epsilon X^{(1)}$ and $\Gamma\simeq\Gamma^{(0)}+\epsilon\Gamma^{(1)}$. The zeroth-order equations are $(X^{(0)})''+X^{(0)}/\Gamma^{(0)}=0$ and $(\Gamma^{(0)})'=0$. With the initial conditions discussed above, the solutions are $X^{(0)}=\cos(\tau+\delta)$ and $\Gamma^{(0)}=1$.

The first-order (in ϵ) equations are

$$(X^{(1)})'' + X^{(1)} - \Gamma^{(1)}\cos(\tau+\delta) = 0, \tag{21}$$

$$(\Gamma^{(1)})' = -2\cos^2(\tau+\delta), \tag{22}$$

with the solutions

$$\Gamma^{(1)} = -\tau + \frac{1}{2}[\sin(2\delta) - \sin(2\tau+2\delta)], \tag{23}$$

$$X^{(1)} = X_A\cos(\tau+\delta) + X_B\sin(\tau+\delta) + \frac{1}{32}\sin[3(\tau+\delta)], \tag{24}$$

where

$$X_A = -\frac{\tau}{8} - \frac{1}{32}\sin(4\delta), \tag{25}$$

$$X_B = \frac{1}{32}\cos(4\delta) + \frac{\tau}{4}\sin(2\delta) - \frac{\tau^2}{4}. \tag{26}$$

Combining the zeroth and first-order solutions yields

$$X = \hat{X}\cos[\tau+\delta-\arctan\Omega], \tag{27}$$

where $\hat{X}=[(1+\epsilon X_A)^2+\epsilon^2X_B^2]^{1/2}$, $\Omega=\epsilon X_B/(1+\epsilon X_A)$, and the third-harmonic term has been neglected. Note that the first-order quantities will remain small, and the above solution valid, provided that $\epsilon\tau^2=(\nu_\gamma t)(\omega_\beta t)\ll 1$. Assuming $\epsilon\tau^2\ll 1$, the above expressions can be expanded to yield

$$x \simeq x_m(1-\nu_\gamma t/8)\cos[(1+\nu_\gamma t/4)\omega_\beta t+\delta], \tag{28}$$

$$\frac{\gamma}{\gamma_0} \simeq 1 - \nu_\gamma t + \frac{1}{2}\frac{\nu_\gamma}{\omega_\beta}[\sin(2\delta) - \sin(2\omega_\beta t+2\delta)]. \tag{29}$$

These equations also imply, to first order in ϵ,

$$u_x \simeq -(\gamma_0 x_m\omega_\beta/c)(1-\nu_\gamma t/2)\sin[(1+\nu_\gamma t/4)\omega_\beta t+\delta]. \tag{30}$$

Time averaging Eq. (29) yields Eq. (12), and, typically, the fast oscillations in the energy evolution can be neglected. The first-order expressions for x and γ given by Eqs. (28) and (29) are adequate for an accurate description of the behavior of a beam, e.g., evolution of the beam emittance and energy spread, as shown below.

B. Electron beam dynamics

In contrast to beam cooling and radiation damping using Thomson scattering [18] or using a magnetic undulator [13], the energy damping of electrons in a plasma focusing channel depends strongly on the radial distribution of the electrons. Specifically, the radiative damping rate is quadratic with respect to the amplitude of the transverse betatron oscillation. Electrons initially injected close to the axis will undergo only very small oscillations and lose almost no energy compared to those injected farther from the axis. This will eventually lead to a significant increase of the energy spread, at least for a radially symmetric beam centered about the axis, which is examined in the following sections.

1. Mean energy

To describe the properties of an electron beam, the appropriate single electron quantities are averaged over an ensemble of beam electrons. For the case of the mean energy of the beam, consider the expression for γ of a single electron given by Eq. (12). Single electron quantities will be expanded about the ensemble averaged value of that quantity plus a small perturbation. For example, the initial energy of a single electron is $\gamma_0=\langle\gamma_0\rangle+\delta\gamma_0$, where the angular brackets denote an ensemble average over the beam, e.g., $\langle\gamma_0\rangle=\Sigma_i\,\gamma_{0i}/N_p$, where γ_{0i} is the initial energy of the ith particle and N_p is the number of particles in the beam. Also, by definition, $\langle\gamma_0\rangle=\langle\gamma\rangle_0$, where $\langle\gamma\rangle_0=\langle\gamma\rangle(t=0)$ and $\langle\gamma\rangle=\Sigma_i\,\gamma_i/N_p$, as well as $\langle\delta\gamma_0^2\rangle=\langle\gamma_0^2\rangle-\langle\gamma_0\rangle^2\equiv\sigma_{\gamma0}^2$, since $\langle\delta\gamma_0\rangle=0$. Similar relations hold for other physical quantities, some details of which are presented in Appendix A.

To the lowest order, assuming that the beam is centered about and injected on axis, the mean energy is

$$\langle\gamma\rangle=\langle\gamma\rangle_0(1+\bar{\nu}_\gamma t)^{-1}, \tag{31}$$

where the mean radiative damping rate is

$$\bar{\nu}_\gamma=\tau_R c^2K^4\langle\gamma\rangle_0\langle x_m^2\rangle/2, \tag{32}$$

with $\langle x_m^2\rangle\simeq\sigma_{x0}^2+c^2\sigma_{ux0}^2/(\bar{\omega}_\beta^2\langle\gamma\rangle_0^2)$ and $\bar{\omega}_\beta=c\bar{k}_\beta=Kc/\langle\gamma\rangle_0^{1/2}$. In terms of the mean betatron strength parameter $\langle a_\beta^2\rangle=\bar{k}_\beta^2\langle\gamma\rangle_0^2\langle x_m^2\rangle$, the mean radiative damping rate is

$$\bar{\nu}_\gamma=\tau_R\omega_\beta^2\langle\gamma\rangle_0\langle a_\beta^2\rangle/2. \tag{33}$$

2. Energy spread

The relative energy spread is $\sigma_\gamma/\langle\gamma\rangle$, where $\sigma_\gamma^2=\langle\delta\gamma^2\rangle=\langle\gamma^2\rangle-\langle\gamma\rangle^2$. To derive an expression for the energy spread, the single electron expression for γ is expanded to second order in the energy perturbation (to $\delta\gamma^2$), and to fourth order for the position and momentum (to δx_0^4 and δu_{x0}^4). The fourth-order development is necessary since the second-order contribution vanishes. The cross-correlation terms (e.g., $\langle\delta x_0\delta\gamma_0\rangle$, etc.) are neglected. Note that for a beam centered about and injected on axis, $x_0=\delta x_0$, $u_{x0}=\delta u_{x0}$, and $\langle x\rangle_0=\langle u_x\rangle_0=0$.

After some algebra (see Appendix A), the normalized energy spread is

$$\frac{\sigma_\gamma^2}{\langle\gamma\rangle^2}\simeq\frac{\sigma_{\gamma0}^2}{\langle\gamma\rangle_0^2}+\frac{1}{2}\tau_R^2c^4K^8\left(\langle\gamma\rangle_0^2\sigma_{x0}^4+\frac{\sigma_{ux0}^4}{K^4}\right)t^2, \tag{34}$$

where Gaussian distributions for the initial positions and momenta are assumed, i.e., $\langle x_0^4\rangle=3\sigma_{x0}^4$. Equation (34) indicates that the energy spread will always increase if the beam is initially centered on axis. This is due to the dependence of the damping on the initial oscillation amplitudes of the electrons (in contrast to the case of radiation via Thomson scattering or from magnetic undulators).

If the beam is initially matched in the channel, such that in the absence of radiation there are no betatron oscillations in the electron beam radial envelope, then $\sigma_{x0}^2=\epsilon_{nx0}/\bar{k}_\beta\langle\gamma\rangle_0$, which implies that $\langle\gamma\rangle_0\sigma_{x0}^2=\sigma_{ux0}^2/K^2$ and $\langle x_m^2\rangle=2\sigma_{x0}^2$. In this case the relative energy spread simplifies to

$$\sigma_\gamma^2/\langle\gamma\rangle^2\simeq\sigma_{\gamma0}^2/\langle\gamma\rangle_0^2+\bar{\nu}_{\gamma m}^2t^2, \tag{35}$$

where $\bar{\nu}_{\gamma m}=\tau_Rc^2K^4\langle\gamma\rangle_0\sigma_{x0}^2$. Note that for the plasma channel in a blown-out regime, $K^2=k_p^2/2$ and $\bar{\nu}_{\gamma m}=\tau_Rc^2k_p^4\langle\gamma\rangle_0\sigma_{x0}^2/4$. Also, for a beam with no initial energy spread ($\sigma_{\gamma0}=0$), $\sigma_\gamma/\langle\gamma\rangle\simeq\bar{\nu}_\gamma t$. This result indicates that the relative energy spread due to the radiation effects for a beam injected on axis will be equal (or greater for a finite initial energy spread) to the relative energy decrease. For example, if the radiation leads to a 10% decrease of the mean beam energy, then the relative energy spread will be at least $\sigma_\gamma/\langle\gamma\rangle\geqslant10\%$.

3. Transverse emittance

The beam radius and momentum follow from Eqs. (28) and (30),

$$\sigma_x^2=\frac{1}{2}\langle x_m^2\rangle-\frac{1}{16}\tau_Rc^2K^4\langle\gamma\rangle_0\langle x_m^4\rangle t, \tag{36}$$

$$\sigma_{ux}^2=\bar{k}_\beta^2\langle\gamma\rangle_0^2\left[\langle x_m^2\rangle-\frac{1}{2}\tau_Rc^2K^4\langle\gamma\rangle_0\langle x_m^4\rangle t\right], \tag{37}$$

where the kurtosis is $\langle x_m^4\rangle\simeq3\sigma_{x0}^4+(2/\bar{k}_\beta^2)\sigma_{x0}^2\sigma_{ux0}^2/\langle\gamma\rangle_0^2+(3/\bar{k}_\beta^4)\sigma_{ux0}^4/\langle\gamma\rangle_0^4$. Neglecting correlations between x and u_x, i.e., $\epsilon_{nx}\simeq\sigma_x\sigma_{ux}$, it can be shown that the normalized transverse emittance of the beam is

$$\epsilon_{nx}\simeq\frac{\bar{k}_\beta\langle\gamma\rangle_0}{2}\langle x_m^2\rangle\left(1-\frac{3}{8}\tau_Rc^2K^4\langle\gamma\rangle_0\frac{\langle x_m^4\rangle}{\langle x_m^2\rangle}t\right). \tag{38}$$

Note that if the beam is initially matched to the plasma channel, then $\sigma_{x0}^2=\epsilon_{nx0}/\langle\gamma\rangle_0\bar{k}_\beta$, which also implies that $\sigma_{x0}=\sigma_{ux0}/\langle\gamma\rangle_0\bar{k}_\beta$. This leads to $\langle x_m^2\rangle=2\sigma_{x0}^2$ and $\langle x_m^4\rangle=8\sigma_{x0}^4$. The expression for the normalized emittance of a matched beam then simplifies to

$$\epsilon_{nx}\simeq\epsilon_{nx0}(1-3\bar{\nu}_{\gamma m}t/2), \tag{39}$$

where $\epsilon_{nx0}=\bar{k}_\beta\langle\gamma_0\rangle\sigma_{x0}^2$ and $\bar{\nu}_{\gamma m}=\tau_Rc^2K^4\langle\gamma\rangle_0\sigma_{x0}^2$.

4. Example

Consider a beam of 1 GeV ($\langle\gamma\rangle_0=2000$), with $\sigma_{\gamma0}/\langle\gamma\rangle_0=1\%$, injected into a blown-out plasma channel

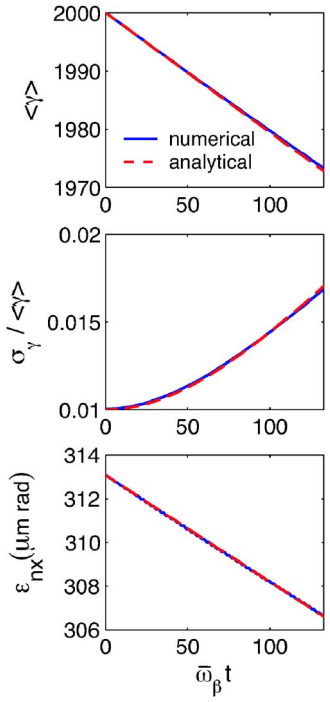

FIG. 1. (Color online) Mean energy, relative energy spread, and normalized transverse emittance (μm rad) for a matched beam with a large initial emittance of 313 μm rad, injected into a blown-out plasma channel with density $n_0=5\times10^{18}$ cm^{-3}. The maximum propagation distance $\bar{\omega}_\beta t_{\max}$ corresponds to a propagation of 2 cm. Plotted are the analytical estimates from Eqs. (31), (35), and (39), and the numerical results from a particle transport code that integrates the single particle equations of motion for a set of 10^5 particles.

with a background electron density $n_0=5\times10^{18}$ cm^{-3}. Because the effect of radiation damping is much stronger for larger beams, as an illustrative example, a very large initial emittance $\epsilon_{nx0}\simeq313$ μm rad is chosen, for which the beam matching condition imposes a relatively large beam radius of 4.86 μm. The mean energy, normalized energy spread, and transverse normalized emittance are shown in Fig. 1, where the analytical estimates from Eqs. (31), (35), and (39) are plotted together with the results from a particle transport code with a set of N_p particles ($N_p=10^5$ in this example). This code integrates the initial set of coupled equations of motion, Eqs. (7) and (8), using a fourth-order Runge-Kutta algorithm. While the mean energy and emittance decrease by only about 1.3% and 2%, respectively, the stronger effect is the evolution of the relative energy spread, which increases by more than 60%. The analytical estimates are in excellent agreement with the numerical solutions.

III. FOCUSING CHANNEL WITH CONSTANT ACCELERATION

In addition to the focusing forces discussed above, this section includes the effects of a constant accelerating force. The accelerating force is assumed to be of the same order as the focusing force, as is typical in plasma-based accelerators. The radiation reaction force is a perturbation in comparison to the accelerating and focusing forces.

It can be shown that the expression of the radiation reaction force remains the same when an accelerating gradient is present. This is because the terms corresponding to the transverse forces dominate the radiation reaction force (cf. Ref. [19]), and whenever the particle is close enough to the channel axis for the focusing force to become too small, the radiation will likewise be negligible.

A. Single particle dynamics

Including the accelerating force into the equations of motion for a single electron gives

$$\dot{x}=cu_x/\gamma\simeq cu_x/u_z, \tag{40}$$

$$\dot{u}_x=-cK^2x-\tau_RK^2c^2u_x(1+K^2\gamma x^2), \tag{41}$$

$$\dot{u}_z=\mathcal{E}-\tau_Rc^2K^4\gamma^2x^2, \tag{42}$$

where $\mathcal{E}=E_{z0}e/mc$ and E_{z0} is the accelerating gradient. In the case of a linear wakefield, $E_{z0}\simeq k_p\phi_0$, or $\mathcal{E}=\omega_p(e\phi_0/mc^2)$. The particle dynamics are described by the following coupled equations,

$$\ddot{x}+\mathcal{E}\dot{x}/\gamma+c^2K^2x/\gamma=0, \tag{43}$$

$$\dot{\gamma}=\mathcal{E}-\tau_Rc^2K^4\gamma^2x^2, \tag{44}$$

which, in terms of normalized quantities, can be written

$$X''+\Lambda X'/\Gamma+X/\Gamma=0, \tag{45}$$

$$\Gamma'=\Lambda-2\epsilon X^2\Gamma^2, \tag{46}$$

where $\Lambda=\mathcal{E}/(\gamma_0\omega_\beta)$.

1. Particle orbits without radiation

As in Sec. II A 3, a time scale separation is assumed $\epsilon\ll1$, allowing the perturbation series: $X\simeq X^{(0)}+\epsilon X^{(1)}$ and $\Gamma\simeq\Gamma^{(0)}+\epsilon\Gamma^{(1)}$. The zeroth-order (without radiation) coupled equations derived from Eqs. (45)–(46) are

$$(X^{(0)})''+\Lambda(X^{(0)})'/\Gamma^{(0)}+X^{(0)}/\Gamma^{(0)}=0, \tag{47}$$

$$(\Gamma^{(0)})'=\Lambda. \tag{48}$$

The solution for the energy evolution is $\Gamma^{(0)}=1+\Lambda\tau$, or $\gamma^{(0)}=\gamma_0+\mathcal{E}t$, i.e., the linear energy increases due to the constant accelerating gradient.

Equation (47) for $X^{(0)}$ can be solved using the WKB method, since the envelope variations are assumed slow compared to the betatron oscillations; the solution is

$$X^{(0)}=(\Gamma^{(0)})^{-1/4}\cos\psi, \tag{49}$$

with $\psi=2(\Gamma^{(0)})^{1/2}/\Lambda-2/\Lambda+\delta$. Equation (49) can be written

$$x=x_m(1+\mathcal{E}t/\gamma_0)^{-1/4}\cos\psi. \tag{50}$$

2. Particle energy with radiative damping

The first-order equation for $\Gamma^{(1)}$, which includes the effects of radiation, is

$$(\Gamma^{(1)})' = -2(X^{(0)}\Gamma^{(0)})^2 = -2(\Gamma^{(0)})^{3/2}\cos^2\psi. \quad (51)$$

As in the previous section, a time averaging over the fast oscillations is performed, which yields $(\Gamma^{(1)})' \simeq -(\Gamma^{(0)})^{3/2}$, with the solution

$$\Gamma^{(1)} \simeq \frac{2}{5\Lambda}[1-(\Gamma^{(0)})^{5/2}]. \quad (52)$$

The time-averaged solution for Γ to first order is then given by $\Gamma \simeq \Gamma^{(0)} + 2\epsilon[1-(\Gamma^{(0)})^{5/2}]/5\Lambda$, or

$$\gamma \simeq \gamma_0 + \mathcal{E}t + \frac{2\nu_\gamma\gamma_0^2}{5\mathcal{E}}\left[1-\left(1+\frac{\mathcal{E}}{\gamma_0}t\right)^{5/2}\right]. \quad (53)$$

Note that, as the acceleration tends to zero, the first-order result of Sec. II A is recovered, $\gamma \simeq \gamma_0(1-\nu_\gamma t)$.

Since the relatively complex source term for the first-order equation for the transverse orbit $X^{(1)}$ did not readily lead to a simple analytical solution, the behavior of X including acceleration, focusing, and radiation is calculated numerically using the particle transport code described above. For this reason, the beam emittance will also be calculated numerically.

B. Electron beam dynamics

Expressions for the beam mean energy and energy spread can be derived analytically, as in the previous section, using a decomposition of the variables into their centroid plus a small deviation.

1. Beam energy

The expression for the mean energy of the beam follows from an ensemble average of the single particle case; this gives

$$\langle\gamma\rangle = \langle\gamma\rangle_0 + \mathcal{E}t + \frac{2}{5}\bar{\nu}_\gamma\frac{\langle\gamma\rangle_0^2}{\mathcal{E}}\left[1-\left(1+\frac{\mathcal{E}}{\langle\gamma\rangle_0}t\right)^{5/2}\right]. \quad (54)$$

Moment calculations provide the following expression for the energy spread, to fourth order in x and u_x (the cross-correlated terms were again neglected):

$$\frac{\sigma_\gamma^2}{\langle\gamma\rangle^2} = (\langle\gamma\rangle_0 + \mathcal{E}t)^{-2}\left\{\sigma_{\gamma 0}^2 + \frac{2\tau_R^2c^4K^8\langle\gamma\rangle_0^4}{25\mathcal{E}^2} \times\left[1-\left(1+\frac{\mathcal{E}t}{\langle\gamma\rangle_0}\right)^{5/2}\right]^2\left(\langle\gamma\rangle_0^2\sigma_{x0}^4 + \frac{\sigma_{ux0}^4}{K^4}\right)\right\}. \quad (55)$$

For a matched beam,

$$\frac{\sigma_\gamma^2}{\langle\gamma\rangle^2} = (\langle\gamma\rangle_0 + \mathcal{E}t)^{-2}\left\{\sigma_{\gamma 0}^2 + \frac{4\bar{\nu}_\gamma^2\langle\gamma\rangle_0^4}{25\mathcal{E}^2}\left[1-\left(1+\frac{\mathcal{E}}{\langle\gamma\rangle_0}t\right)^{5/2}\right]^2\right\}. \quad (56)$$

And, for early times, $\mathcal{E}t/\langle\gamma\rangle_0 \ll 1$,

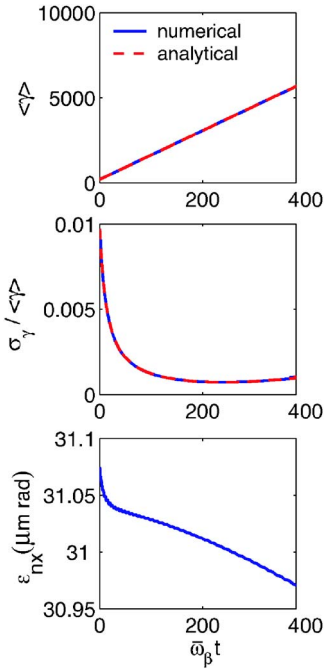

FIG. 2. (Color online) Mean energy, relative energy spread, and normalized transverse emittance (μm rad) for a 100 MeV beam injected into a 2 cm long, blown-out plasma channel ($n_0 = 5\times10^{18}$ cm^{-3}) with a constant acceleration $E_{z0} = 150$ GV/m. The solid blue curves represent the numerical calculations from the particle transport code, while the dashed red curves (for $\langle\gamma\rangle$ and $\sigma_\gamma/\langle\gamma\rangle$) are the analytical estimates Eqs. (54) and (55).

$$\frac{\sigma_\gamma^2}{\langle\gamma\rangle^2} = \langle\gamma\rangle_0\left(1-2\mathcal{E}t/\langle\gamma\rangle_0\right)\left(\sigma_{\gamma 0}^2 + \langle\gamma\rangle_0^2\bar{\nu}_\gamma^2t^2\right). \quad (57)$$

Initially, the spread decreases linearly with time due to the linear increase of the zeroth-order mean energy. For later times, $t^2 > \sigma_{\gamma 0}^2/(\langle\gamma\rangle_0^2\bar{\nu}_\gamma^2)$, the energy spread can increase due to the effects of radiation.

2. Laser wakefield accelerator example

Consider the case of an electron beam typical of that produced by a 100 MeV-class laser wakefield accelerator ($\langle\gamma\rangle_0 = 200$, $\sigma_{\gamma 0}/\langle\gamma\rangle_0 = 1\%$, $\epsilon_{nx0} \simeq 31$ μm), injected into a blown-out plasma channel with a constant longitudinal acceleration. The plasma density is 5×10^{18} cm^{-3}, the channel width is 20 μm, and the accelerating gradient is 150 GV/m, which would correspond to a typical laser wakefield with $a_0 \simeq 1$ (where a_0 is the normalized vector potential of the laser). The beam radius is initially matched to the plasma channel, which corresponds to $\sigma_{x0} = 2.7$ μm. These parameters are typical of present experiments that aim at achieving an acceleration of multi-GeV electrons using a several cm long plasma channel (such as a capillary discharge). The results are shown in Fig. 2. The total propagation length corresponds to 2 cm. Over the first millimeters of propagation, the energy spread decreases as $\propto 1/t$ due to the dominant linear increase of the mean energy. However, after about 1 cm (or $\bar{\omega}_\beta t \simeq 200$), the spread starts to increase due to the radiation effects. The analytical estimates from Eqs. (54) and

(55) are plotted in Fig. 2, as well as the result from the particle transport code [numerical solution to the single particle equations of motion Eqs. (41) and (42) for 10^5 particles]. Analytical estimates for the mean energy and relative energy spread are in excellent agreement with the numerical results.

It should also be noted that with these parameters (and in particular this plasma density), uniform acceleration of the electrons could not be maintained for such long distances in a single acceleration stage due to the dephasing effect. It is well-known that in plasma accelerators, the electrons can outrun the phase velocity of the wake, which is roughly equal to the velocity of the drive beam (e.g., the group velocity of the laser) in the plasma and hence smaller than c. The dephasing length is given approximately by $L_{\mathrm{deph}} \simeq \lambda_p \omega_0^2 / 2\omega_p^2$, where λ_p is the plasma wavelength, ω_0 the laser frequency, and ω_p the plasma frequency. One solution to dephasing is to use multiple stages in which the plasma channels are separated by a drift section and are placed such as to reposition the electrons in the proper phase in the wakefield. Alternatively, the dephasing length in a single stage using an axially uniform plasma density can be increased by reducing the plasma density. For the above parameters, $L_{\mathrm{deph}} \simeq 2.5$ mm, so the negative effects of the radiation on the energy spread should not have the time to occur before the dephasing length is reached in a single stage.

3. Plasma wakefield accelerator example

The effects of radiation can be more important in plasma wakefield accelerators that are driven by highly relativistic electron beams. In this case, the acceleration distance is typically not limited by dephasing, but rather by some other constraint, such as the length of the plasma or the propagation distance of the electron beam. One effect that can limit the propagation distance of the drive beam is depletion of the drive beam energy. Since the decelerating field inside the bunch is typically on the order of the accelerating field behind the bunch, this can be roughly estimated by dividing the energy of the drive beam by the accelerating field of the wake. For example, if a 30 GeV electron beam is used to drive a wake of amplitude 10 GV/m, then the driven beam propagation can be expected to be altered after a depletion distance on the order of 3 m.

As an illustrative example in which the effects of radiation are significant, consider a 30 GeV beam propagating in a blown-out plasma channel with a density of 3×10^{17} cm^{-3} [5], a constant acceleration gradient of 37 GV/m, and a beam with an initial radius $\sigma_{x0} = 10$ μm. The results are shown in Fig. 3. The maximum propagation length on these figures, with the chosen normalization, corresponds to 30 cm. In addition to the sudden growth of the emittance due to the mismatched beam (the detailed analytical treatment of the mismatched beam case is presented in the Appendix B), the energy spread strongly increases due to the radiation. For a variety of small initial energy spreads (in this particular example we chose $\sigma_{\gamma 0} = 10^{-3} \langle \gamma \rangle_0$), after 30 cm the energy spread is close to 10%. Note also that because the radiation effect is not sufficiently small for this example (i.e., $\epsilon \tau^2 \sim 1$), the first-order analytical model starts to fail describing the energy spread at longer times.

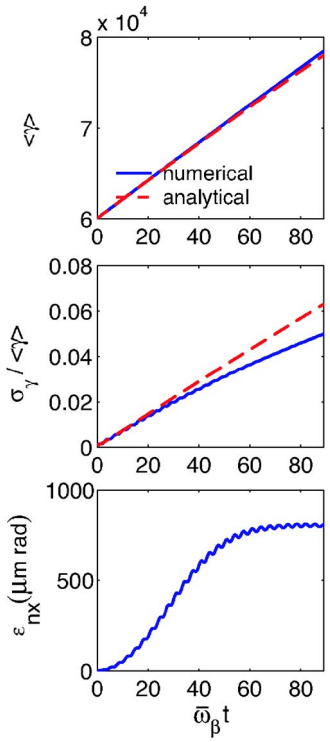

FIG. 3. (Color online) Mean energy, relative energy spread, and normalized transverse emittance (μm rad) for a 30 GeV beam injected into a 30 cm long blown-out plasma channel with a constant acceleration gradient of 37 GV/m and a density $n_0 = 3 \times 10^{17}$ cm^{-3}. The solid blue curves represent the numerical calculations from the particle transport code, while the dashed red curves (for $\langle \gamma \rangle$ and $\sigma_\gamma / \langle \gamma \rangle$) are the analytical estimates Eqs. (54) and (55).

Next, consider a similar case but with a lower plasma density. All the parameters remain the same except for $n_0 = 10^{16}$ cm^{-3}, e.g., the propagation length is still 30 cm. However, the 30 cm of propagation now correspond to much fewer betatron oscillations (about 15, compared to almost 100 in the previous case with $n_0 = 3 \times 10^{17}$ cm^{-3}), hence the effect of radiation is much smaller. In particular, the energy spread does not increase, but on the contrary, exhibits a decrease due to the acceleration as shown in Fig. 4. Furthermore, although the matching condition is not quite fulfilled yet, the emittance does not have the time to grow to large values.

These examples indicate that the effects of the radiation could be significant for the beam quality in plasma wakefield acceleration experiments. In addition to radiation lowering the energy gain (as discussed in Ref. [12]), radiation could strongly affect the energy spread due to the quadratic dependence of the radiation damping on the betatron oscillation amplitude. This effect could be controlled, however, by an appropriate choice of beam and plasma parameters, such that the amplitude and number of betatron oscillations remain small.

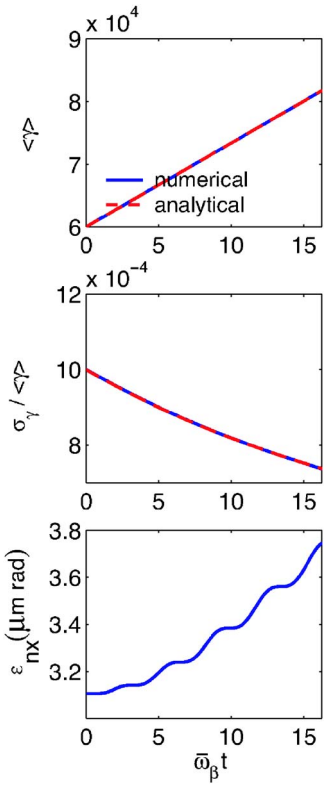

FIG. 4. (Color online) Mean energy, relative energy spread, and normalized transverse emittance (μm rad) for a 30 GeV beam injected into a 30 cm long blown-out plasma channel with a constant acceleration gradient of 37 GV/m and a density $n_0=10^{16}$ cm^{-3}. The solid blue curves represent the numerical calculations from the particle transport code, while the dashed red curves (for $\langle\gamma\rangle$ and $\sigma_\gamma/\langle\gamma\rangle$) are the analytical estimates Eqs. (54) and (55).

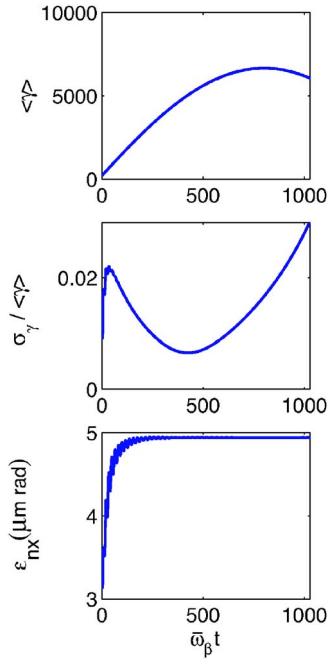

FIG. 5. (Color online) Mean energy, relative energy spread, and normalized transverse emittance (in m rad) for a 100 MeV beam injected into a 20 cm long plasma wakefield accelerator with a density $n_0=3\times10^{17}$ cm^{-3}.

IV. BEAM DYNAMICS IN A PLASMA WAKEFIELD

If the fields that apply onto the particles are known analytically, then we can derive a set of coupled equations describing the motion of the single particles, such as Eqs. (7) and (8), that can be solved numerically for a variety of analytically specified focusing and accelerating fields. As discussed previously, the equations of motion for a set of test particles were solved numerically using a particle transport code based on a fourth-order Runge-Kutta algorithm. Here, electron beam evolution including the effects of radiation is examined for the case in which the focusing and accelerating fields are described by linear plasma wakefield theory.

For a drive laser pulse with a Gaussian radial intensity profile, linear theory predicts that the resulting plasma wakefield is described by an electrostatic potential of the form

$$\Phi = \Phi_0 \exp(-x^2/x_c^2)\cos k_p(z-v_p t), \tag{58}$$

where Φ is the electrostatic potential normalized to e/mc^2 and $v_p \simeq v_g = c(1-\omega_p^2/\omega_0^2)^{1/2}$ is the phase velocity of the wake, which is approximately equal to the group velocity v_g of the laser pulse (with frequency ω_0) propagating in the plasma. With this form for the wakefield, the Lorentz equation, neglecting the radiation reaction force, is $d\boldsymbol{u}/dct = \boldsymbol{\nabla}\Phi$.

By treating the radiation reaction force as a perturbation, the electron motion can be described by the following coupled equations: $\dot{x}=cu_x/\gamma$, $\dot{z}=cu_z/\gamma$,

$$\dot{u}_x = \frac{-2c\Phi_0}{x_c^2} x \exp\left(-\frac{x^2}{x_c^2}\right)\cos[k_p(z-v_p t)] - \frac{4\tau_R c^2 \Phi_0^2}{x_c^4}\gamma u_x \times \exp\left(-\frac{x^2}{x_c^2}\right)\cos^2[k_p(z-v_p t)], \tag{59}$$

and

$$\dot{u}_z = -ck_p\Phi_0\left(1-\frac{x^2}{x_c^2}\right)\exp\left(-\frac{x^2}{x_c^2}\right)\sin[k_p(z-v_p t)] - \frac{4\tau_R c^2\Phi_0^2}{x_c^4}\gamma^2 x^2 \exp\left(-\frac{x^2}{x_c^2}\right)\cos^2[k_p(z-v_p t)]. \tag{60}$$

The unperturbed expressions for the focusing and accelerating forces show that there is a phase region of length $\lambda_p/4$ where the electrons will undergo both focusing and acceleration. This limits the actual dephasing length (for both acceleration and focusing) to half the one-dimensional value, i.e., $L_{\mathrm{deph}} \simeq \gamma_p^2 \lambda_p/2$, where $\gamma_p=(1-v_p^2/c^2)^{-1/2}=\omega_0/\omega_p$ is the relativistic Lorentz factor associated with phase velocity of the wakefield.

As an example, consider parameters that are typical of experiments on the next generation of a GeV-class laser wakefield accelerators. The plasma has a relatively low density ($n_0=3\times10^{17}$ cm^{-3}) and is sufficiently long (20 cm) to provide a strong acceleration of the injected beam before the dephasing length is reached (i.e., when the electron overtakes the wake and begins to decelerate). The laser wavelength is

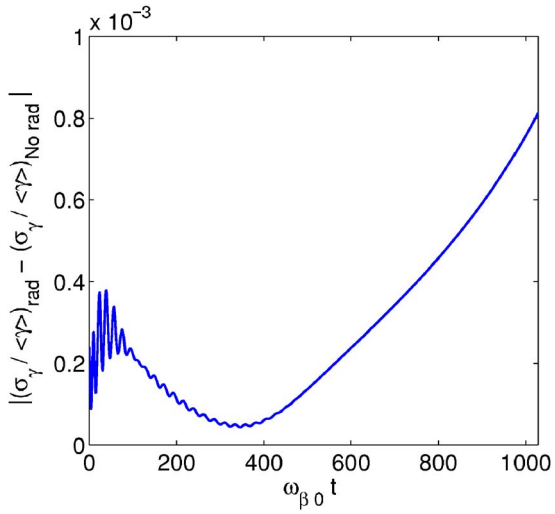

FIG. 6. (Color online) Difference between the relative energy spread with and without radiation reaction, for the parameters of Fig. 5.

$\lambda_0=0.8$ μm (Ti:Sapphire laser system), with a spot size of 20 μm (rms) and a normalized electric field of $a_0=1$, where $a_0 \simeq 0.85\times 10^{-9}\lambda_0[\mu\text{m}](I[\text{W/cm}^2])^{1/2}$ with I the laser intensity. The electron beam injected into the wakefield has an initial normalized transverse emittance of $\epsilon_{nx0}\simeq 3$ μm, an initial energy of nearly 100 MeV ($\langle\gamma_0\rangle=200$), an rms energy spread of 1%, and is focused to the initially matched radius of 1.75 μm. The initial electron bunch length is $\sigma_{z0}=0.1$ μm. These are typical parameters for a plasma generated in a capillary discharge, which would provide a guiding of the laser pulse, even at high intensities, to compensate for the natural diffraction length of the laser.

The numerical results from the transport code (with 10^5 particles) are shown in Fig. 5. The plasma length has been chosen slightly longer than the dephasing length to illustrate the dephasing effect. The effective dephasing length here is $L_{\text{deph}}=\gamma_p^2\lambda_p/2\simeq 17.7$ cm, which is close to the propagation length from injection to the maximum energy in this example (the bunch is injected close to the defocusing region, with a bunch length sufficiently short such that all the electrons are accelerated and focused). The electron beam reaches a maximum energy of about 3.4 GeV after about 15 cm of propagation. The energy spread decreases to its minimum just before the maximum energy is reached. This is due to the rotation of the electron bunch in phase space as it is accelerated along trapped orbits. With these parameters, the difference in energy spread for the cases with and without radiation reaction is only of the order 10^{-4} (cf. Fig. 6), which is negligible. This shows that even for rather optimistic laser wakefield accelerator parameters, the dephasing should occur before the radiation effects become significant. To reach high energies in a single stage with an axial uniform plasma requires the use of low plasma densities (in order to avoid dephasing). Lower plasma densities imply less betatron oscillations and consequently a smaller radiation effect.

V. DISCUSSION AND CONCLUSIONS

The effects of radiation reaction on the electron beam evolution in plasma-based accelerators has been examined analytically and with the use of test particle simulations. In this study, the radiation is a result of the betatron motion of the beam electrons due to the focusing fields of the plasma, and the effects of the radiation on the beam were modeled using the classical radiation reaction force. A variety of cases were examined, including beam evolution in a plasma focusing channel with and without a constant accelerating field, as well as the case of focusing and accelerating fields as described by linear wakefield theory. In general, radiation decreases the energy gain, the emittance (if the beam is initially matched in the channel) and, more importantly, increases the relative energy spread of the beam. It should also be noted that the analytical formalism presented here is general and can be applied to any straight system with linear focusing forces.

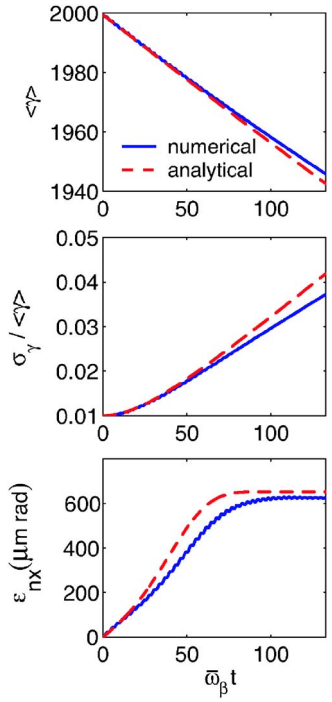

FIG. 7. (Color online) Mean energy, relative energy spread, and normalized transverse emittance (μm rad) for a large mismatched beam injected on axis into a blown-out plasma channel. The dashed red curves are the analytical estimates Eqs. (A2), (A4), and (B12). The solid blue curves are the numerical results from the particle transport code (using 10^5 particles).

The effects of radiation on the electron beam are determined by the characteristic time scale $\bar{\nu}_\gamma^{-1}$, where $\bar{\nu}_\gamma$ is the mean radiative damping rate given by Eq. (32). For example, in a plasma focusing channel in the absence of acceleration, the mean energy of the beam decreases as $(1+\bar{\nu}_\gamma t)^{-1}$, as in Eq. (31), whereas for a matched beam, the energy spread of the beam increases asymptotically as $\bar{\nu}_\gamma t$, as in Eq. (35), and the beam emittance decreases linearly with $\bar{\nu}_\gamma t$, as in Eq. (39). In terms of the mean betatron wavelength, $\bar{\lambda}_\beta=2\pi\langle\gamma\rangle_0^{1/2}/K$, the mean radiative damping factor for a matched beam is

$$\bar{\nu}_\gamma t=(16\pi^3/3)r_e\langle\gamma\rangle_0^2\epsilon_{nx0}z/\bar{\lambda}_\beta^3, \tag{61}$$

where r_e is the classical electron radius. In practical units,

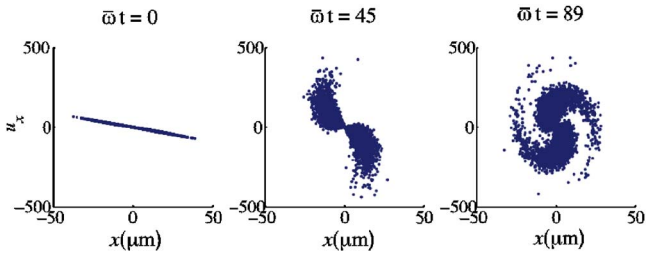

FIG. 8. (Color online) Transverse phase space (x, u_x) at $\bar{\omega}_\beta t=0$, $\bar{\omega}_\beta t=45$, and $\bar{\omega}_\beta t=89$, for a large mismatched beam injected on axis into a blown-out plasma channel.

$$\bar{\nu}_\gamma t = 4.7 \times 10^{-7} \langle \gamma \rangle_0^2 (\epsilon_{nx0}[\mu\mathrm{m}])(\bar{\lambda}_\beta[\mu\mathrm{m}])^{-2}(z/\bar{\lambda}_\beta). \quad (62)$$

Note that in the blowout regime $\bar{\lambda}_\beta=(2\langle\gamma\rangle_0)^{1/2}\lambda_p$.

As an example, consider parameters relevant to experiments on the plasma wakefield accelerator in the blowout regime using a 28.5 GeV electron beam [5]: $\langle\gamma\rangle_0=5.6\times10^4$, $n_0=2.8\times10^{17}$ cm^{-3}, $\lambda_p=62$ μm, $\bar{\lambda}_\beta=2.1$ cm, and $\sigma_{x0}=10$ μm. Note that the matched emittance for the $\sigma_{x0}=10$ μm beam in the blowout channel is $\epsilon_{nx0}=2\pi\langle\gamma\rangle_0\sigma_{x0}^2/\bar{\lambda}_\beta=1.7$ mm, which is relatively large. Assuming $z=10\bar{\lambda}_\beta$, these parameters give $\bar{\nu}_\gamma t=5.7\times10^{-2}$. This implies, for example, that the normalized energy spread would grow to at least 5.7%, even if the beam had initially zero energy spread. The reason for this relatively large value of $\bar{\nu}_\gamma t$ is that the matched emittance is large due to an assumed matched beam radius of $\sigma_{x0}=10$ μm.

Highly relativistic electron beams of this class can have a much lower emittance, e.g., $\epsilon_{nx0}=10$ μm, than assumed in the above example. However, matching such a beam into a channel with such strong focusing would require a very small beam radius, e.g., $\sigma_{x0}=0.78$ μm. This would result in a much smaller value of $\bar{\nu}_\gamma t=3.3\times10^{-4}$. Injecting such a radially small beam is problematic and would require very strong focusing prior to injection into the plasma channel. Note that if a beam of $\epsilon_{nx0}=10$ μm is injected at 28.5 GeV into a channel with $\bar{\lambda}_\beta=2.1$ cm at a more typical radius of $\sigma_{x0}=10$ μm, it would be highly mismatched and the beam emittance would grow towards the matched value. Once the emittance has reached its matched value, the beam parameters would evolve according to the equations describing the matched beam evolution. The time scale for the emittance to grow to its matched value is determined by the decoherence time, t_{dc}, as discussed in Appendix B. For early times, $t \ll t_{dc}$, the emittance blow-up due to phase mixing will be small, and the changes to the energy spread can be small. For a sufficiently large initial energy spread satisfying $\sigma_{\gamma0}/\langle\gamma\rangle_0 \gg (\pi\bar{\nu}_\gamma/\omega_\beta)^{1/2}$, the decoherence time is $t_{dc}\simeq\pi\langle\gamma_0\rangle/(\omega_\beta\sigma_{\gamma0})$. For a sufficiently small initial energy spread satisfying $\sigma_{\gamma0}/\langle\gamma\rangle_0 \ll (\pi\bar{\nu}_\gamma/\omega_\beta)^{1/2}$, the decoherence time is $t_{dc}\simeq(2\pi/\omega_\beta\bar{\nu}_\gamma)^{1/2}$.

The situation is somewhat different for laser wakefield accelerators. Typically, the accelerated bunch in a laser wakefield accelerator is produced from self-trapping and evolves in such a manner that it is approximately self-matched at a small radius in the focusing fields of the wake. As noted above, the relevant scale for the acceleration length is the dephasing length, $L_{\mathrm{deph}}=\lambda_p^3/2\lambda_0^2$. In terms of the acceleration distance normalized to L_{deph}, the quantity $\bar{\nu}_\gamma t$ can be written

$$\bar{\nu}_\gamma t = (2^{3/2}\pi^3/3) r_e \langle\gamma\rangle_0^{1/2} \epsilon_{nx0} \lambda_0^{-2} (z/L_{\mathrm{deph}}), \quad (63)$$

or in practical units,

$$\bar{\nu}_\gamma t = 8.2 \times 10^{-8} \langle\gamma\rangle_0^{1/2} (\epsilon_{nx0}[\mu\mathrm{m}])(\lambda_0[\mu\mathrm{m}])^{-2}(z/L_{\mathrm{deph}}). \quad (64)$$

As an example, consider a 2 GeV ($\langle\gamma\rangle_0=4\times10^3$) laser wakefield accelerator in the blowout regime with a density $n_0=5\times10^{17}$ cm^{-3}, $\lambda_p=47$ μm, $\bar{\lambda}_\beta=0.42$ cm, $\lambda_0=0.8$ μm, $\epsilon_{nx0}=10$ μm, and a matched bunch radius of $\sigma_{x0}=1.3$ μm. After a single stage ($z=L_{\mathrm{deph}}$), $\bar{\nu}_\gamma t=8.1\times10^{-5}$. Again, here the effects of radiation on the electron bunch are small, due to the small transverse size of the bunch.

The above expressions rigorously describe the effects of radiation on electron beams that are initially matched in the focusing channel, neglecting the effects of acceleration, as presented in Sec. II. These results have been generalized to include the effects of a constant accelerating field (Sec. III), and test particle simulations have been presented to study the case in which the focusing and accelerating fields represent those derived from linear plasma wakefield theory (Sec. IV). The case of mismatched beams has been described in Appendix B and studied with test particle simulations.

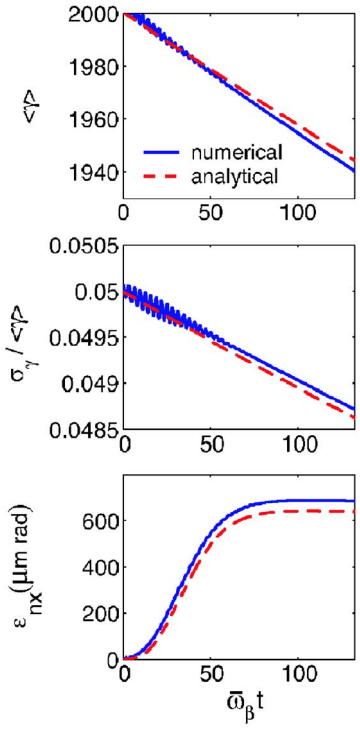

FIG. 9. (Color online) Mean energy, relative energy spread, and normalized transverse emittance (μm rad) for a narrow, mismatched beam injected off axis into a blown-out plasma channel. The dashed red curves are the analytical estimates from Eqs. (A2), (B13), and (B12), and the solid blue curves are the numerical results from the particle transport code (using 10^5 particles).

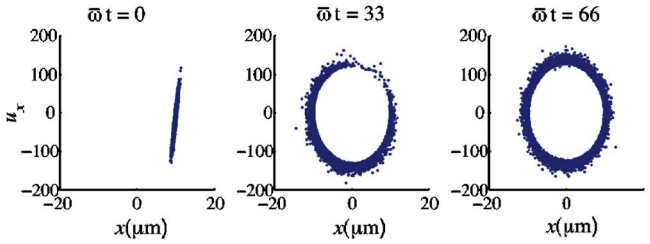

FIG. 10. (Color online) Transverse phase space (x, u_x) at $\bar{\omega}_\beta t=0$, $\bar{\omega}_\beta t=33$, and $\bar{\omega}_\beta t=66$, for a narrow beam injected off axis into a blown-out plasma channel.

Generally, injecting a beam with a spot size larger than the matched radius into a plasma channel, may lead to large betatron oscillations, and to a quick growth of the emittance towards its matched value. The resulting radiation can then significantly affect the beam, inducing a relative energy spread that can be on the several percent level. This can have detrimental effects on applications such as for high-energy physics and free electron lasers operating in the x-ray regime, which require high quality electron beams with energy spreads on the order of a fraction of a percent.

On the other hand, provided that the beam is initially matched in the channel at typical values of a normalized emittance ($\epsilon_{nx0}\sim 10$ μm or less), the effects of radiation on the beam are not important. This is because a matched beam at typical values of $\epsilon_{nx0}\sim 10$ μm has a very small radius, and consequently the betatron oscillation, as well as the resulting radiation, is small. As noted above, this can be challenging, due to the relatively large focusing fields required to focus the beam into such plasma channels. The matched beam radius is $\sigma_{x0}^2=\epsilon_{nx0}\bar{\lambda}_\beta/2\pi\langle\gamma\rangle_0\sim\epsilon_{nx0}(\langle\gamma\rangle_0 n_0)^{-1/2}$. For example, a 2 GeV electron beam with $\epsilon_{nx0}=10$ μm in a blowout plasma with $n_0=10^{18}$ cm^{-3} has a matched radius of $\sigma_{x0}\sim 1$ μm. Injecting such a small beam into the channel will require very strong focusing prior to the channel, perhaps requiring the use of a novel mechanism such as a plasma lens.

ACKNOWLEDGMENTS

The authors gratefully acknowledge discussions with Patric Muggli and Estelle Michel. This work was supported by U.S. Department of Energy, Office of Science, Contract No. DE-AC02-05CH11231.

APPENDIX A: GENERAL EXPRESSION FOR THE MEAN ENERGY AND ENERGY SPREAD

In this appendix, a general expression is derived for the relative energy spread, valid for a matched or mismatched beam, injected on axis ($\langle x_0\rangle=0$) or off axis ($\langle x_0\rangle\neq 0$). The assumptions made are (i) $\langle u_x\rangle_0=0$ (i.e., the beam is injected straight into the channel), (ii) the distributions contain only even moments (e.g., $\langle\delta x_0^3\rangle=0$), and (iii) there are no initial correlations in the beam distribution.

The single particle energy Eq. (12) with the radiative damping rate ν_γ Eq. (13) is

$$\gamma=\gamma_0\left[1+\frac{1}{2}\tau_R c^2K^4\left(\gamma_0 x_0^2+\frac{u_{x0}^2}{K^2}\right)\right]^{-1}. \tag{A1}$$

Quantities are written in terms of the centroid and a deviation, i.e., $\gamma_0=\langle\gamma\rangle_0+\delta\gamma_0$, $x_0=\langle x\rangle_0+\delta x_0$, and $u_{x0}=\delta u_{x0}$. A series is developed for the different moment orders and consideration is given to the possible off-axis initial condition $\langle x\rangle_0=0$. Owing to vanishing second-order moments, the lowest-order radiative correction to the energy spread requires development to fourth order (e.g., σ_{x0}^4).

The expression for the mean energy, neglecting the third-order and higher terms is

$$\langle\gamma\rangle=\frac{\langle\gamma\rangle_0}{B}\left[1-\frac{At}{B}\left(\frac{\langle x\rangle_0^2}{\langle\gamma\rangle_0}\sigma_{\gamma0}^2-\langle\gamma\rangle_0\sigma_{x0}^2-\frac{\sigma_{ux0}^2}{K^2}\right)\right], \tag{A2}$$

where $A=\tau_R c^2K^4/2$ and $B=1+A\langle\gamma\rangle_0\langle x\rangle_0^2 t$. This expression includes the second-order moments, including a possible off-axis initial condition. The fourth-order expression for the standard deviation $\sigma_\gamma^2=\langle\gamma^2\rangle-\langle\gamma\rangle^2$ is

$$\sigma_\gamma^2=\frac{\sigma_{\gamma0}^2}{B^4}-\frac{A}{B^3}\sigma_{\gamma0}^2\left(4\langle\gamma\rangle_0\sigma_{x0}^2+\frac{2}{K^2}\sigma_{ux0}^2\right)+\frac{A^2}{B^4}\Bigg[2t^2\langle x\rangle_0^2\big(\sigma_{\gamma0}^4+2\langle\gamma\rangle_0^4\sigma_{x0}^2\big)+t^2\langle\gamma_0^4\rangle\big(\langle\delta x_0^4\rangle-\sigma_{x0}^4\big)-\frac{1}{K^4}\big(\langle\gamma\rangle_0^2\sigma_{ux0}^4+4\langle\gamma\rangle_0^3\sigma_{x0}^2\sigma_{ux0}^2\big)\Bigg]. \tag{A3}$$

Note that, when $\langle x\rangle_0=0$, the second-order moment contributions vanish. If the distribution for x_0 is Gaussian, then $\langle\delta x_0^4\rangle=3\sigma_{x0}^4$. The relative energy spread is

$$\frac{\sigma_\gamma^2}{\langle\gamma\rangle^2}\simeq\frac{\sigma_{\gamma0}^2+\tau_R^2c^4K^8\langle\gamma\rangle_0^4\langle x\rangle_0^2\sigma_{x0}^2t^2+\frac{1}{2}\tau_R^2c^4K^8\langle\gamma\rangle_0^4\sigma_{x0}^4t^2+\frac{1}{2}\tau_R^2c^4K^4\langle\gamma\rangle_0^2\sigma_{ux0}^4t^2}{\langle\gamma\rangle_0^2\big(1+\frac{1}{2}\tau_Rc^2K^4\langle\gamma\rangle_0\langle x\rangle_0^2t\big)^2}. \tag{A4}$$

APPENDIX B: MISMATCHED BEAMS

Consider a beam that is not initially matched in the plasma channel. If the beam is initially mismatched and has a finite energy spread, then different particles among the beam will undergo betatron oscillations at different frequencies, $\omega_\beta\propto\gamma^{-1/2}$. This will lead to a slippage of the particles with respect to each other, and to emittance growth, until the emittance reaches the matched value. In this appendix, the

beam decoherence time (i.e., the time at which the slippage between the particles becomes significant) is calculated, as well as the emittance evolution, for a mismatched beam. Also analyzed is the energy spread for narrow beam injected off axis, including a description of the conditions necessary for reduction in the energy spread. Note that in the following, the decoherence time is assumed to be much smaller that the radiation damping time.

1. Beam decoherence

An approximate method for estimating the decoherence time consists of considering two particles in the beam with energies at the two ends of the distribution: $\gamma_1=\langle\gamma\rangle+\sigma_\gamma$ and $\gamma_2=\langle\gamma\rangle-\sigma_\gamma$. The phase associated with the betatron oscillations of these two particles is

$$\varphi_{1,2}=\int dt\omega_{\beta 1,2}, \tag{B1}$$

where $\omega_{\beta 1,2}=Kc/\gamma_{1,2}^{1/2}$. The phase terms can be expanded using $\gamma_{1,2}=\langle\gamma\rangle\pm\sigma_\gamma$ with $\sigma_\gamma^2/\langle\gamma\rangle^2\ll 1$, which yields

$$\Delta\varphi\simeq\omega_\beta\int dt\sigma_\gamma/\langle\gamma\rangle, \tag{B2}$$

where $\Delta\varphi=\varphi_1-\varphi_2$.

Consider the case in which the initial energy spread is greater than that induced by radiation, i.e., $\sigma_{\gamma 0}^2/\langle\gamma\rangle_0^2\gg\bar{\nu}_\gamma^2 t^2$. In this case $\sigma_\gamma/\langle\gamma\rangle\simeq\sigma_{\gamma 0}/\langle\gamma\rangle_0$ and $\Delta\varphi\simeq\omega_\beta t\sigma_{\gamma 0}/\langle\gamma\rangle_0$. The decoherence time t_{dc} can be defined as the time when the phase difference between the low energy part of the beam and the high energy part is π, i.e., $\Delta\varphi(t=t_{dc})=\pi$. This gives

$$t_{dc}\simeq\frac{\pi\langle\gamma\rangle_0}{\omega_\beta\sigma_{\gamma 0}}. \tag{B3}$$

Note that the initial energy spread will determine the coherence time provided $\sigma_{\gamma 0}^2/\langle\gamma\rangle_0^2\gg\bar{\nu}_\gamma^2 t_{dc}^2$, which gives $\sigma_{\gamma 0}^2/\langle\gamma\rangle_0^2\gg\pi\bar{\nu}_\gamma/\omega_\beta$.

Consider the opposite limit, in which the initial energy spread is smaller than that induced by radiation, i.e., $\sigma_{\gamma 0}^2/\langle\gamma\rangle_0^2\ll\bar{\nu}_\gamma^2 t^2$. In this case $\sigma_\gamma/\langle\gamma\rangle\simeq\bar{\nu}_\gamma t$ and $\Delta\varphi\simeq\omega_\beta\bar{\nu}_\gamma t^2/2$. The decoherence time is then

$$t_{dc}\simeq\left(\frac{2\pi}{\omega_\beta\bar{\nu}_\gamma}\right)^{1/2}. \tag{B4}$$

Radiation induced energy spread will determine the decoherence time provided $\sigma_{\gamma 0}^2/\langle\gamma\rangle_0^2\ll 2\pi\bar{\nu}_\gamma/\omega_\beta$.

2. Emittance growth

The decoherence of the beam eventually leads to a growth of the emittance, which grows until saturation at the matched value. The evolution of the emittance can be examined by considering the electron orbits in the absence of radiation effects, i.e., the case in which decoherence is dominated by the initial energy spread, as discussed above. Consider the electron orbits

$$x=x_m\cos\Psi, \tag{B5}$$

$$u_x=u_{xm}\sin\Psi, \tag{B6}$$

with $\Psi=\omega_\beta t$, $u_{xm}=-\gamma_0\omega_\beta x_m/c$, and $u_{xm}^2=K^2\gamma_0 x_0^2+u_{x0}^2$.

Since the emittance growth effect considered here is purely due to phase mixing, the oscillation amplitudes are assumed to be the centroid values (or standard deviations in the case where the centroid is zero), i.e., $\langle x^2\rangle\simeq\langle x_0^2\rangle\langle\cos^2\Psi\rangle$, etc. This gives

$$\langle\delta x^2\rangle=\frac{\langle x_m^2\rangle}{2}[1+\langle\cos 2\Psi\rangle]-\langle x_m\rangle^2\langle\cos\Psi\rangle^2, \tag{B7}$$

$$\langle\delta u_x^2\rangle=\frac{\langle u_{xm}^2\rangle}{2}[1-\langle\cos 2\Psi\rangle]-\langle u_{xm}\rangle^2\langle\sin\Psi\rangle^2, \tag{B8}$$

$$\begin{aligned}\langle\delta x\delta u_x\rangle^2=&\frac{\langle x_m u_{xm}\rangle^2}{4}\langle\sin 2\Psi\rangle^2\\&-\langle x_m u_{xm}\rangle\langle x_m\rangle\langle u_{xm}\rangle\langle\sin 2\Psi\rangle\\&\times\langle\cos\Psi\rangle\langle\sin\Psi\rangle\\&+\langle x_m\rangle^2\langle u_{xm}\rangle^2\langle\cos\Psi\rangle^2\langle\sin\Psi\rangle^2.\end{aligned} \tag{B9}$$

Assuming $\gamma_0\simeq\langle\gamma_0\rangle$ in the amplitude terms leads to simplifications in these expressions, i.e., $\langle x_m u_{xm}\rangle^2=\langle x_m^2\rangle\times\langle u_{xm}^2\rangle$, $\langle u_{xm}^2\rangle=K^2\langle\gamma_0\rangle\langle x_m^2\rangle$, and $\langle u_{xm}\rangle^2=K^2\langle\gamma_0\rangle\langle x_m\rangle^2$.

The sinusoidal terms in the above equations can be approximated by assuming that the energy distribution about the mean energy is initially Gaussian and remains so during the beam propagation. The width σ_γ and mean energy γ are allowed to vary, but the $\delta\gamma=\gamma-\langle\gamma\rangle$ distribution is assumed to not deviate too far from a Gaussian. To proceed, the energy is expanded about its mean value to first order in $\delta\gamma/\langle\gamma\rangle$, i.e., $\gamma=\langle\gamma\rangle+\delta\gamma$, $\omega_\beta\simeq\bar{\omega}_\beta(1-\delta\gamma/2\langle\gamma\rangle)$ (where $\omega_\beta=Kc/\gamma^{1/2}$ and $\bar{\omega}_\beta=Kc/\langle\gamma\rangle_0^{1/2}$), and $\Psi\simeq\bar{\omega}_\beta t(1-\delta\gamma/2\langle\gamma\rangle)$. The ensemble averaged quantities can then be expressed as averages over the distribution of energy deviations, e.g.,

$$\begin{aligned}\langle\cos\Psi\rangle&\simeq\frac{1}{\sigma_\gamma\sqrt{2\pi}}\int_{-\infty}^{\infty}d\delta\gamma\exp(-\delta\gamma^2/2\sigma_\gamma^2)\cos(\Psi_0+\delta\Psi)\\&=\exp(-\nu_\epsilon^2 t^2)\cos\Psi_0,\end{aligned} \tag{B10}$$

where $\Psi_0=\bar{\omega}_\beta t$ and $\delta\Psi=-\Psi_0\delta\gamma/2\langle\gamma\rangle$, and

$$\nu_\epsilon=\frac{\bar{\omega}_\beta\sigma_\gamma}{\sqrt{8}\langle\gamma\rangle}. \tag{B11}$$

Similar expressions involving averages over the fast oscillations can be derived: $\langle\sin\Psi\rangle=\exp(-\nu_\epsilon^2 t^2)\sin\Psi_0$, $\langle\sin 2\Psi\rangle=\exp(-4\nu_\epsilon^2 t^2)\sin 2\Psi_0$, and $\langle\cos 2\Psi\rangle=\exp(-4\nu_\epsilon^2 t^2)\cos 2\Psi_0$. Note that the exponent recovers the approximate expression of the decoherence time given above in the limit that decoherence is dominated by the initial energy spread: $\nu_\epsilon\simeq 1/t_{dc}$.

The transverse normalized emittance can be calculated using the definition $\epsilon_{nx}^2=\langle\delta x^2\rangle\langle\delta u_x^2\rangle-\langle\delta x\delta u_x\rangle^2$, which gives

$$\epsilon_{nx}^2=\frac{K^2\langle\gamma\rangle_0}{4}\left(1-\frac{3}{4}\tau_R c^2K^4\langle\gamma\rangle_0\frac{\langle x_m^4\rangle}{\langle x_m^2\rangle}t\right)[\langle x_m^2\rangle^2(1-e^{-8\nu_\epsilon^2t^2})-2\langle x_m^2\rangle\langle x\rangle_m^2(e^{-2\nu_\epsilon^2t^2}-e^{-6\nu_\epsilon^2t^2})]. \tag{B12}$$

The factor $[1-(3/4)\tau_R c^2K^4\langle\gamma\rangle_0\langle x_m^4\rangle t/\langle x_m^2\rangle]$ in Eq. (B12) accounts for the effects of radiation damping, which was assumed to occur on a time scale long compared to that of decoherence. Note that for long times, $\nu_\epsilon^2t^2\gg1$, this reduces to the previous expression Eq. (38).

3. Narrow beam injected off axis

Consider the case of a narrow beam injected off axis. This case can be analyzed using the expression for the energy spread derived in Appendix A with $\langle x\rangle_0\neq0$. Neglecting the fourth-order terms gives

$$\frac{\sigma_\gamma}{\langle\gamma\rangle}\simeq\frac{(\sigma_{\gamma0}^2+4\bar{\nu}_{\gamma\mathrm{on}}\bar{\nu}_{\gamma\mathrm{off}}\langle\gamma\rangle_0^2t^2)^{1/2}}{\langle\gamma_0\rangle(1+\bar{\nu}_{\gamma\mathrm{off}}t)}, \tag{B13}$$

where $\bar{\nu}_{\gamma\mathrm{off}}=\tau_R c^2K^4\langle\gamma\rangle_0\langle x\rangle_0^2/2$ (energy damping rate for a beam injected off axis) and $\bar{\nu}_{\gamma\mathrm{on}}=\tau_R c^2K^4\langle\gamma\rangle_0\sigma_{x0}^2/2$ (energy damping rate for a beam injected on axis).

For this case, the energy spread is no longer unconditionally increasing. In particular, the time derivative of the relative energy spread is

$$\frac{d}{dt}\frac{\sigma_\gamma}{\langle\gamma\rangle}=\frac{\bar{\nu}_{\gamma\mathrm{off}}}{\langle\gamma_0\rangle(1+\bar{\nu}_{\gamma\mathrm{off}}t)^2}\frac{4\bar{\nu}_{\gamma\mathrm{on}}\langle\gamma_0\rangle^2t-\sigma_{\gamma0}^2}{(\sigma_{\gamma0}^2+4\bar{\nu}_{\gamma\mathrm{off}}\bar{\nu}_{\gamma\mathrm{on}}\langle\gamma_0\rangle^2t^2)^{1/2}}. \tag{B14}$$

The relative energy spread will first decrease, but will then increase after a time t_{crit} given by

$$t_{\mathrm{crit}}=\frac{\sigma_{\gamma0}^2}{4\bar{\nu}_{\gamma\mathrm{on}}\langle\gamma_0\rangle^2}. \tag{B15}$$

Likewise, the relative energy spread is at its minimum when $t=t_{\mathrm{crit}}$.

By examining the relative energy spread at its minimum value ($t=t_{\mathrm{crit}}$), a range can be defined for which the decrease in the energy spread is significant. This range is defined by the inequalities $\sigma_{\gamma0}^2>4\bar{\nu}_{\gamma\mathrm{on}}\bar{\nu}_{\gamma\mathrm{off}}\langle\gamma_0\rangle^2t_{\mathrm{crit}}^2$ and $1<\bar{\nu}_{\gamma\mathrm{off}}t_{\mathrm{crit}}$. These inequalities imply

$$\frac{2\sigma_{x0}}{\langle x_0\rangle}<\frac{\sigma_{\gamma0}}{\langle\gamma_0\rangle}<\frac{2\langle x_0\rangle}{\sigma_{x0}}. \tag{B16}$$

This can be satisfied when $\sigma_{x0}\ll\langle x_0\rangle$, i.e., a significant decrease in energy spread is possible for a very narrow beam with a sufficient energy spread injected sufficiently far from the channel axis.

4. Examples

First, consider the case of a mismatched beam injected on axis. A blown-out plasma channel is assumed with a background plasma density of $n_0=5\times10^{18}$ cm^{-3} and a channel width $x_c=30$ μm, along with an injected beam of energy 1 GeV ($\langle\gamma\rangle_0=2000$, $\sigma_{\gamma0}/\langle\gamma\rangle_0=1\%$) with a radius $\sigma_{x0}=10$ μm and an initial emittance of 3.1 μm. Shown in Fig. 7 are the analytical estimates (dashed red curves) Eqs. (A2), (A4), and (B12), and the numerical results (solid blue curves) from the particle transport code (using 10^5 particles). After 2 cm of propagation, the mean energy decreases by less than 3%. However, the effect of the radiation on the energy spread is quite dramatic, with an increase by a factor of four. The emittance quickly grows at the beginning, until it reaches the matched value and starts to slowly decrease due to radiative effects. The analytical estimates are in reasonably good agreement with the results of the particle transport code, although the strong radiation leads to an error between the analytical and numerical curves (at longer times, the perturbation theory begins to break down). Note that, in this particular case, the growth of the cross correlation between the particles' energies and their transverse position and momentum can also contribute to the mismatch. Indeed, after some propagation the particles near the axis in (x,u_x) phase space will not radiate significant energy, while those the farther from the axis will radiate a significant amount of energy. The mean energy loss is approximately four times larger than the initial energy spread, and, hence, the correlated energy spread will grow larger than the initial, uncorrelated energy spread.

Figure 8 shows the phase space (x,u_x) for three different times as obtained from the particle transport code for the same parameters as Fig. 7. The physical process (phase mixing) leading to the emittance growth is clearly illustrated.

Next, consider the case of off-axis injection of a very narrow beam with a rather large energy spread: $\langle x\rangle_0=10$ μm, $\sigma_{x0}=0.1$ μm, and $\sigma_{\gamma0}/\langle\gamma\rangle_0=5\%$ (such that $\sigma_{\gamma0}/\langle\gamma\rangle_0>\sigma_{x0}/\langle x\rangle_0$). The other parameters remain the same as in the previous example. The numerical results from the particle transport code (with 10^5 particles) are shown in Fig. 9. As predicted by Eqs. (B13) and (B12), the energy spread decreases; however, the emittance exhibits extreme growth, by a factor $\simeq200$, due to phase mixing. The growth in transverse emittance due to phase mixing for this example is shown in Fig. 10.

[1] E. Esarey, P. Sprangle, J. Krall, and A. Ting, IEEE Trans. Plasma Sci. **24**, 252 (1996).
[2] C. G. R. Geddes, C. Toth, J. van Tilborg, E. Esarey, C. B. Schroeder, D. Bruhwiler, C. Nieter, J. Cary, and W. P. Leemans, Nature (London) **431**, 538 (2004).
[3] S. P. D. Mangles, C. D. Murphy, Z. Najmudim, A. G. R. Thomas, J. L. Collier, A. E. Dangor, E. J. Divall, P. S. Foster, J. G. Gallacher, C. J. Hooker *et al.*, Nature (London) **431**, 535 (2004).
[4] J. Faure, Y. Glinec, A. Pukhov, S. Kiselev, S. Gordienko, E. Lefebvre, J. P. Rousseau, F. Burgy, and V. Malka, Nature (London) **431**, 541 (2004).
[5] M. J. Hogan *et al.*, Phys. Rev. Lett. **95**, 054802 (2005).
[6] E. Esarey, B. A. Shadwick, P. Catravas, and W. P. Leemans, Phys. Rev. E **65**, 056505 (2002).
[7] A. Rousse, K. T. Phuoc, R. Shah, A. Pukhov, E. Lefebvre, V. Malka, S. Kiselev, F. Burgy, J.-P. Rousseau, D. Umstadter *et al.*, Phys. Rev. Lett. **93**, 135005 (2004).
[8] K. T. Phuoc, F. Burgy, J.-P. Rousseau, V. Malka, A. Rousse, R. Shah, D. Umstadter, A. Pukhov, and S. Kiselev, Phys. Plasmas **12**, 023101 (2005).
[9] S. Wang, C. E. Clayton, B. E. Blue, E. S. Dodd, K. A. Marsh, W. B. Mori, C. Joshi, S. Lee, P. Muggli, T. Katsouleas *et al.*, Phys. Rev. Lett. **88**, 135004 (2002).
[10] C. E. Clayton, B. E. Blue, E. S. Dodd, C. Joshi, K. A. Marsh, W. B. Mori, S. Wang, P. Catravas, S. Chattopadhyay, E. Esarey *et al.*, Phys. Rev. Lett. **88**, 154801 (2002).
[11] W. A. Barletta, E. P. Lee, R. Bonifacio, and L. D. Salvo, Nucl. Instrum. Methods Phys. Res. A **423**, 256 (1999).
[12] D. K. Johnson *et al.*, in *Proceedings of the 2005 Particle Accelerator Conference* (IEEE, New Jersey, 2005), pp. 1625–1627.
[13] *Handbook of Accelerator Physics and Engineering*, edited by A. W. Chao and M. Tigner (World Scientific, Singapore, 1999).
[14] A. Baurichter *et al.*, Phys. Rev. Lett. **79**, 3415 (1997).
[15] P. Sprangle and E. Esarey, Phys. Fluids B **4**, 2241 (1992).
[16] V. Telnov, Phys. Rev. Lett. **78**, 4757 (1997).
[17] Z. Huang and R. D. Ruth, Phys. Rev. Lett. **80**, 976 (1998).
[18] E. Esarey, Nucl. Instrum. Methods Phys. Res. A **455**, 7 (2000).
[19] J. D. Jackson, *Classical Electrodynamics* 3rd ed. (Wiley, New York, 1999).
[20] Z. Huang and R. D. Ruth, in *Proceedings of the 1999 Particle Accelerator Conference* (IEEE, New Jersey, 1999), pp. 262–266.
[21] M. Reiser, *Theory and Design of Charged Particle Beams* (Wiley, New York,1994).